ISSN 1063-7761, Journal of Experimental and Theoretical Physics, 2018, Vol. 126, No. 2, pp. 217–223. © Pleiades Publishing, Inc., 2018.
Original Russian Text © Yu.S. Orlov, V.A. Dudnikov, M.S. Platunov, M.V. Gorev, D.A. Velikanov, N.V. Kazak, S.Yu. Gavrilkin, L.A. Solov'ev, A.A. Veligzhanin, S.N. Vereshchagin, S.G. Ovchinnikov, 2018, published in Zhurnal Eksperimental'noi i Teoreticheskoi Fiziki, 2018, Vol. 153, No. 2, pp. 259–267.

ORDER, DISORDER, AND PHASE TRANSITION IN CONDENSED SYSTEM

Low-Temperature Schottky Anomalies and the Magnetic State of the *p* Electrons of Oxygen in Substituted $Gd_{0.4}Sr_{0.6}CoO_{3-\delta}$ Cobaltites

Yu. S. Orlov[a,b,*], V. A. Dudnikov[a], M. S. Platunov[a], M. V. Gorev[a], D. A. Velikanov[a], N. V. Kazak[a], S. Yu. Gavrilkin[c], L. A. Solov'ev[d], A. A. Veligzhanin[e], S. N. Vereshchagin[d], and S. G. Ovchinnikov[a]

[a] *Kirensky Institute of Physics, Siberian Branch, Russian Academy of Sciences, ul. Akademgorodok 50/38, Krasnoyarsk, 660036 Russia*

[b] *Siberian Federal University, Krasnoyarsk, 660041 Russia*

[c] *Lebedev Physical Institute, Russian Academy of Sciences, Moscow, 119991 Russia*

[d] *Institute of Chemistry and Chemical Technology, Siberian Branch, Russian Academy of Sciences, ul. Akademgorodok 50/24, Krasnoyarsk, 660036 Russia*

[e] *Russian Research Centre "Kurchatov Institute," pl. Kurchatova 1, Moscow, 123182 Russia*

**e-mail: jso.krasn@mail.ru*

Received June 22, 2017

Abstract—The XANES spectra (X-ray absorption near-edge spectra) at the *K* edge of Co and the L_3 edge of Gd in polycrystalline $Gd_{0.4}Sr_{0.6}CoO_{3-\delta}$ rare-earth oxides with an ordered and disordered distribution of Gd^{3+} and Sr^{2+} cations over the *A* sites in the crystal lattice are measured. The results of XANES measurements do not reveal a noticeable shift in the absorption edge with increasing Sr concentration as compared to the $GdCoO_3$ parent composition. The measured temperature dependences of the heat capacity of polycrystalline ordered and disordered samples and a single-crystal ordered $Gd_{0.4}Sr_{0.6}CoO_{2.85}$ sample exhibit two Schottky anomalies. These anomalies are thought to be related to the high-spin state of the Co^{3+} ions in the pyramidal environment caused by oxygen deficiency and to the magnetic state of oxygen *p* electrons induced by the doping-assisted generation of a hole in the 2*p* state. The absence of a noticeable shift in the absorption edge and the presence of two Schottky anomalies support the fact that the charge state of cobalt remains unchanged in the compounds under study.

DOI: 10.1134/S1063776118020036

1. INTRODUCTION

The rare-earth cobalt oxides $RCoO_3$ (*R* is a rare-earth ion) doped with divalent alkali metals form a class of materials with unique physical properties [1]. Like supercooling La_2CuO_4 cuprates and $RMnO_3$ manganites, they belong to systems with strong electron correlations and are insulators in the plain state. However, the cobaltites have a specific feature caused by the competition of the spin states of the Co^{3+} ion. The filling of the d^6 electron shell of the Co^{3+} ion does not obey the Hund rules and the ground state is represented by a low-spin (LS) term with $S = 0$ rather than a high-spin (HS) state with spin $S = 2$. Doping is a fundamental method to control many physical properties of complex oxides, and the balance between the one-site interaction energy and the charge transfer energy can strongly affect an electronic structure according to the nature of the unsubstituted ground state [2, 3]. For example, doping in the Mott–Hubbard dielectric mode directly changes the valence state of transition metal ions (manganite case), and doping in the charge-transfer dielectric mode leads to the appearance of carriers in the oxygen sublattice (cuprate case). Cobaltites are likely to belong to the transition (crossover) region between these two limiting cases. A detailed understanding of the formation of this crossover region can eventually answer the question why complex oxide cobaltites exhibit such unusual magnetic and electronic properties, which has attracted the attention of researchers for several decades [4].

As in manganites, hole doping in cobaltites causes conduction and the formation of a magnetic order. The traditional concept of the appearance of ferromagnetism consists in a change in the charge state of cobalt ions, which results in exchange interaction between aliovalent ions in terms of the double

Table 1. Designation, lattice, and nonstoichiometry δ of polycrystalline $Gd_{0.4}Sr_{0.6}CoO_{3-\delta}$ samples (298 K)

Composition	State	Designation	Lattice	δ
$Gd_{0.4}Sr_{0.6}Co$	Ordered	GSC-ord	Tetragonal	0.22
$O_{3-\delta}$	Disordered	GSC-dis	Cubic	0.36

exchange model. The substitution of alkaline earth metal ions for some rare-earth ions gives rise to localized holes. In this case, the properties of a system are considered in terms of a state with a mixed valence of Co^{3+} and Co^{4+} ions, and the fraction of Co^{4+} ions increases monotonically with the degree of doping [5–7].

However, other standpoints regarding the valence of cobalt in such compounds exist. Using the $Sm_{1-x}Ca_xCoO_{3-\delta}$ compound as an example, the authors of [8] showed that the removal of every oxygen ion during synthesis at normal oxygen pressure decreases the local coordination of transition metal ions from octahedral to pyramidal without changing the valence of cobalt. At a low temperature, the Co^{3+} ions in the pyramidal environment are in a magnetic state. In [9], we studied substituted cobaltites using a $Gd_{0.4}Sr_{0.6}CoO_{2.85}$ single crystal as an example. An analysis of the XANES spectra at the edges of the Co and Gd ions did not support the assumption about the appearance of Co^{4+} ions upon hole doping and points to a more complex nature of the hole states at the top of the valence band formed by the hybridized *p* states of oxygen and the 3*d* states of cobalt.

In this work, we measure XANES spectra at the *K* edge of Co and the L_3 edge of Gd in ceramic $Gd_{0.4}Sr_{0.6}CoO_{3-\delta}$ oxides with ordered and disordered cation Gd^{3+} and Sr^{2+} distributions over the *A* sites in their crystal lattice and determine the temperature dependence of the heat capacity C_P of these oxides and an ordered $Gd_{0.4}Sr_{0.6}CoO_{2.85}$ single crystal. The measured XANES spectra have a specific feature that is identical to that of the single crystal, and the low-temperature part of the heat capacity has two Schottky anomalies. These anomalies are thought to be related to the HS state of the Co^{3+} ions in the pyramidal environment caused by oxygen deficiency and to the magnetic state of oxygen *p* electrons, which is induced by the doping-assisted generation of a hole in the 2*p* state.

2. EXPERIMENTAL

Polycrystalline $Gd_{0.4}Sr_{0.6}CoO_{3-\delta}$ samples were prepared using a standard ceramic technology from the stoichiometric amounts of Gd_2O_3 (99.9% purity), Co_3O_4 (99.7%), and $SrCO_3$ (99%). They were thoroughly mixed with ethanol in a jasper mortar, and the prepared mixture was annealed in air at 1473 K for 12 h. Pressed pellets were annealed under the same conditions for 16 h. *A*-site-ordered (GSC-ord) samples were fabricated by cooling to room temperature at a rate of 2 K/min, and *A*-site-disordered (GSC-dis) samples were fabricated by cooling from the synthesis temperature to room temperature at a rate of 100 K/s. No air annealing at $T = 773$ K was performed to achieve the maximum oxygen nonstoichiometry.

X-ray diffraction (XRD) analysis was carried out on a PANalyticalX'Pert PRO diffractometer (CoK_α radiation) in the angular range $2\theta = 10°–140°$, and X-ray diffraction patterns at high temperatures were recorded using a high-temperature AntonPaar HTK 1200N chamber. XRD results were processed by the Rietveld full-profile analysis of polycrystals [10] and minimizing the derivative of the difference [11].

The oxygen contents in the $Gd_{0.4}Sr_{0.6}CoO_{3-\delta}$ samples were determined from the sample mass loss during hydrogen reduction according to the technique from [12], the error of determining nonstoichiometry δ was ±0.01, and the results are given in Table 1.

XANES (X-ray absorption near-edge) and EXAFS (extended X-ray absorption fine structure) spectra were measured at the *K* edge of Co and the L_3 edge of Gd in $Gd_{1-x}Sr_xCoO_{3-\delta}$ on the CTM station (K1.3b) of the Russian Research Centre Kurchatov Institute. Absorption spectra were recorded in transmission geometry at room temperature. As a monochromator, we used a Si(111) single crystal with a slit, which ensured an energy resolution $\Delta E/E \sim 2 \times 10^{-4}$. The scanning step in the XANES region was about 0.4 eV and the counting time was 4 s per point.

The heat capacity was measured on the PPMS Quantum Design (United States) device equipped with a special-purpose unit and located at the Center for Collective Use of the Lebedev Physical Institute.

The magnetization was measured on an MPMS-XL Quantum Design SQUID magnetometer.

3. RESULTS AND DISCUSSION

At temperatures above 1473 K, the samples consisted of Sr/Gd-cation-disordered nonstoichiometric cubic perovskites (Figs. 1c, 2b). An exothermic process was detected upon slow cooling (2 K/min) in the temperature range 1263–1363 K, and this process can be attributed to the phase transition of cubic perovskite into its tetragonal modification with the formation of a superstructure with an ordered arrangement of Sr/Gd cations and anion vacancies (Figs. 1a, 2a). The reverse transition of the tetragonal ordered phase into the cubic phase occurred upon heating in the temperature range 1273–1403 K. On fast cooling (about 100 K/s) from $T = 1473$ K, the samples retained a cubic structure with a uniform random distribution of Sr/Gd cations and anion vacancies (Figs. 1b, 2b), and the quenched metastable state remained unchanged in air at temperatures below 1073 K.

Figure 3 shows the normalized XANES spectra of $GdCoO_3$, ordered $Gd_{0.4}Sr_{0.6}CoO_{2.78}$, and disordered $Gd_{0.4}Sr_{0.6}CoO_{2.64}$ measured at the K edge of Co at room temperature. The absorption maximum (at about 7727 eV) corresponds to the dipole-allowed $1s$–$4p$ transition [13]. No significant shift of the absorption edge of Co is observed when Sr substitutes for gadolinium. The energy position of the absorption edge ($E_0 = 7724$ eV) for the substituted samples is close to the absorption edge of $GdCoO_3$ (Co^{3+}). The found value of E_0 agrees with the data determined for plain $LaCoO_3$ and $EuCoO_3$ cobaltites [13–15]. A shift of the absorption K edge toward high energy is thought to indicate an increase in the absorbing-atom charge. For example, the shift at the K edge of Co induced by the substitution of Co^{3+} for Co^{2+} is about 3 eV (Fig. 3, upper panel) [16]. The absence of such a shift in the case of $GdCoO_3$, GSC-ord, and GSC-dis demonstrates that the charge state of Co remains unchanged. Such an effect was observed earlier in $La_{1-x}Sr_xCoO_{3\pm\delta}$ perovskites [14, 17–19]. The substitution of Sr^{2+} ions for Gd^{3+} ions could lead to an increase in the charge of Co ($Co^{3+} \rightarrow Co^{4+}$) or the appearance of holes at oxygen. The second scenario of hole doping, where holes are more strongly localized at the O($2p$) states, is likely to take place in the $Gd_{1-x}Sr_xCoO_{3-\delta}$ system. In this case, the Co($3d$) states and, hence, the charge state of cobalt should change weakly. The holes at the O($2p$) states will be charge carriers and the interaction of unpaired oxygen spins with the cobalt subsystem can give an additional contribution to magnetism. The appearance of holes at oxygen in the $La_{1-x}Sr_xCoO_{3\pm\delta}$ system was experimentally supported by the XANES and XMCD spectra measured at the K edge of O in [18, 20]. It was also shown that the addition of Sr led to the shift of the K edge of O toward low energy and to a change in the absorption intensity. A significant increase in the XMCD signal, which was related to the appearance of a nonzero orbital magnetic moment at oxygen, was detected in [21].

The substitution of Sr^{2+} ions for some Gd^{3+} ions changes the shape and the intensity of the near-edge region, the maximum of which shifts toward low energy (to about 7711.2 eV). This behavior can be explained by a change in the spin state of the Co^{3+} ions in the Sr-substituted sample. A change in the spin state (LS or HS) creates unfilled t_{2g} states and gives rise to a redistribution of the $1s$–$3d$ transition intensities, which is accompanied by a shift of the center of the near-edge feature toward low energy [17, 22].

The influence of Sr substitution on the local electronic structure of Gd was studied by measuring XANES spectra at the L_3 edge of Gd. Figure 4 shows the XANES spectra of $GdCoO_3$, GSC-ord, GSC-dis, and Gd_2O_3 (taken as a standard of Gd^{3+}). The energy maximum at 7248 eV is related to the $2p_{3/2}$–$5d$ dipole

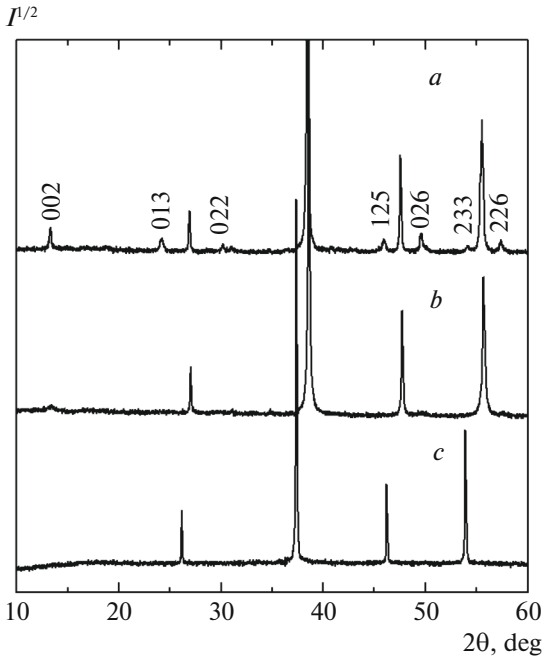

Fig. 1. Fragments of the X-ray diffraction patterns of (a) annealed CGS-ord (ordered) and (b) quenched GSC-dis (disordered) samples at (b) room temperature and (c) 1200°C. (b, c) Fundamental reflections of cubic perovskite. (a) Superlattice reflections of tetragonal perovskite. The indices of the reflections of (b, c) cubic structure from left to right are 100, 110, 111, and 200; the weakest reflection is 100 and the strongest reflection is 110. (a) $I4/mmm$, $Z = 16$, $a = 7.6785(2)$ Å, $c = 15.398(5)$ Å, $V = 907.87(5)$ Å^3; (b) $Pm3m$, $Z = 1$, $a = 3.83421(6)$ Å, $V = 56.367(3)$ Å^3; and (c) $Pm3m$, $Z = 1$, $a = 3.94640(5)$ Å, $V = 61.462(2)$ Å^3.

transition of the Gd^{3+} ion ($4f^7$). The introduction of Sr increases the transition intensity, which can be associated with both an increase in the number of unfilled $5d$ states and a change in the degree of Gd($5d$)–O($2p$) hybridization.

The results of XANES measurements demonstrate that, as the Sr^{2+} content increases, (i) the absorption K edge of Co does not shift (which can indicate that the charge state of Co does not change (Co^{3+})), (ii) the holes at the $2p$ states of oxygen can contribute to the magnetic state of the system along with Gd^{3+} and Co^{3+} ions, and (iii) the holes at the O($2p$) states hybridized with the Gd($5d$) states can increase the number of unoccupied $5d$ states.

The temperature dependences of the molar heat capacities of the ordered $Gd_{0.4}Sr_{0.6}CoO_{2.85}$ single crystal and the ordered/disordered $Gd_{0.4}Sr_{0.6}CoO_{3-\delta}$ polycrystalline samples did not exhibit significant differences in the temperature range under study ($T < 275$ K). Therefore, as an example, we only show the experimental temperature dependence of the heat capacity of the $Gd_{0.4}Sr_{0.6}CoO_{2.85}$ single crystal (Fig. 5,

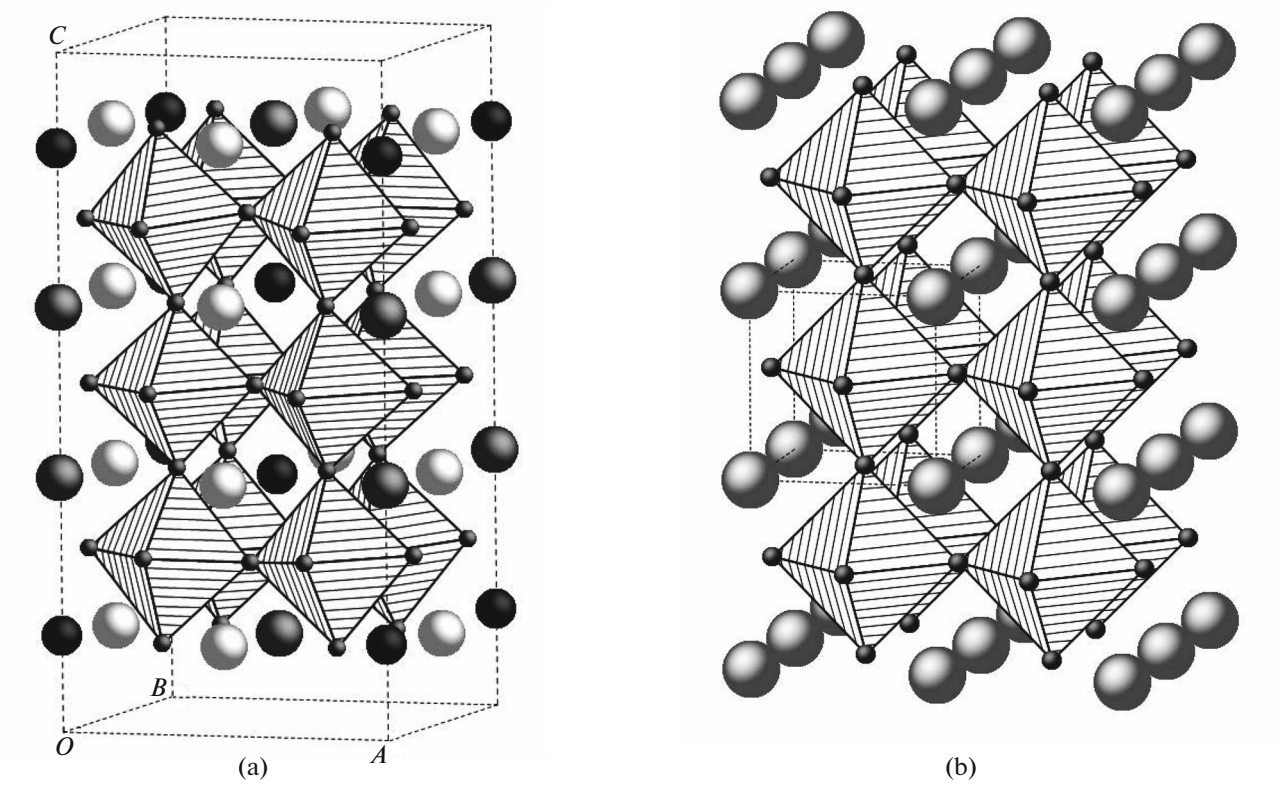

Fig. 2. Structures of (a) *A*-site-ordered (GSC-ord) and (b) *A*-site-disordered (GSC-dis) perovskites $Gd_{0.4}Sr_{0.6}CoO_{2.78}$ and $Gd_{0.4}Sr_{0.6}CoO_{2.64}$, respectively. (dashed lines) Unit cells of their crystal lattices. Octahedra correspond to the position of Co^{3+} with O^{2-} anions at the vertices and spheres are Sr^{2+} and Gd^{3+} cations. (a) Small black spheres are Sr^{2+} or Gd^{3+}, large gray and light gray spheres are crystallographically different Sr^{2+} sites. (b) Light gray spheres indicate the sites statistically occupied by Sr^{2+}/Gd^{3+} cations.

open circles). Specific features at a low temperature and $T \approx 125$ K are clearly visible (Fig. 5a). The latter feature is caused by a transition into a paramagnetic state (Fig. 6). To determine the characteristics related to these features, we divided the molar heat capacity into a regular component (lattice and electronic) C_r and anomalous contribution ΔC. To determine the contribution of the anharmonic component and free electrons to the heat capacity, we used a linear combination of the Debye and Einstein functions with an additional linear term,

$$C_r(T) = aC_D(T) + bC_E(T) + cT.$$

The results for $C_r(T)$ are illustrated as the dashed line in Fig. 5 (Debye temperature is $T_D = 267.4$ K, Einstein temperature is $T_E = 578$ K). Anomalous contribution ΔC is shown in the inset to Fig. 5a.

The heat capacity at low temperatures $T < 30$ K (Figs. 5b, 5c) was processed as the sum (solid curve) of the heat capacities of electrons, lattice, and two Schottky heat capacity contributions (Figs. 5b, 5c; dotted curve),

$$C_p = C_r(T) + K_1C_{SH1}(T, \Delta_1) + K_2C_{SH2}(T, \Delta_2),$$

where

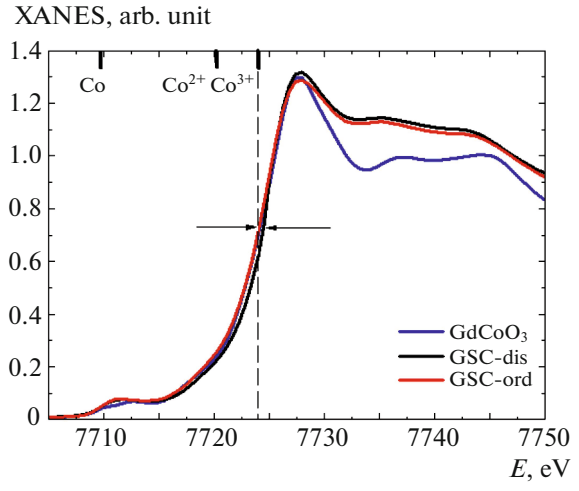

Fig. 3. (Color online) Co *K*-edge XANES spectra of $GdCoO_3$ and $Gd_{0.4}Sr_{0.6}CoO_{3-\delta}$ (GSC).

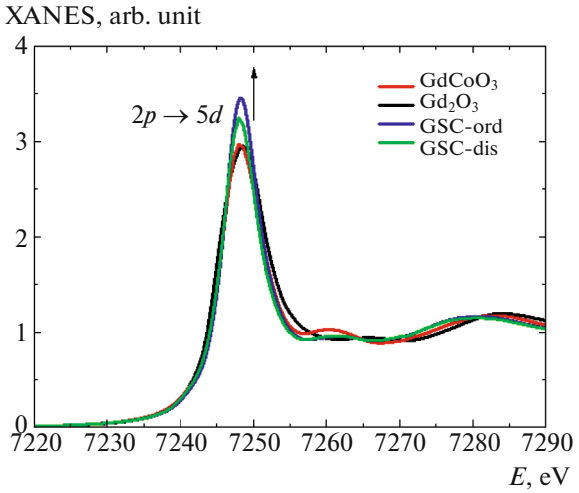

Fig. 4. (Color online) Gd L_3-edge XANES spectra of $GdCoO_3$ and $Gd_{0.4}Sr_{0.6}CoO_{3-\delta}$ (GSC) in comparison with a Gd_2O_3 standard ($T = 300$ K).

$$C_{SH}(T,\Delta) = NR\left(\frac{\Delta}{k_BT}\right)^2 g\frac{\exp(\Delta/k_BT)}{[1+g\exp(\Delta/k_BT)]^2},$$

Δ is the energy range between the ground state and the nearest excited state, R is the molar gas constant, k_B is the Boltzmann constant, N is the concentration of ions with a two-level structure, and g is the degeneracy multiplicity of the ground and the excited states. The relation $C_r(T) = cT + AT^3$ was used in the low-temperature range. The cubic term is a long-wavelength approximation for the Debye model. In this temperature range, this approximation describes the heat capacity of the lattice best of all [23].

Figure 5b shows the simulation results for the case of when only gap is used, $\Delta_1 = \Delta = 12.75$ K and $\Delta_2 = 0$. The best agreement with the experimental data (Fig. 5c) is achieved at $g = 2$ in the presence of exactly two Schottky anomalies corresponding to two energy gaps, $\Delta_1 = 8.3$ K and $\Delta_2 = 21.8$ K (Fig. 5c, dotted curve). In both cases concentration N is fixed and corresponds to the component composition and the oxygen nonstoichiometry of $Gd_{0.4}Sr_{0.6}CoO_{2.85}$.

The nature of formation of the first energy gap Δ_1 can be understood using the following concept: some Co^{3+} ions is in pyramidal environment in the HS state ($^5T_{2g}$) [24] with an effective orbital moment $L = 1$ and spin $S = 2$ because of oxygen deficiency. As a result of spin–orbit coupling, the ground state is represented by a state with a total angular moment $J = 1$, which is split by the crystal field into a singly degenerate state with an angular moment projection $J_z = 0$ and a doubly degenerate state with projection $J_z = \pm 1$ the energy of which is higher by Δ_1 (Fig. 7a). These considerations correspond to the analogous conclusions drawn in

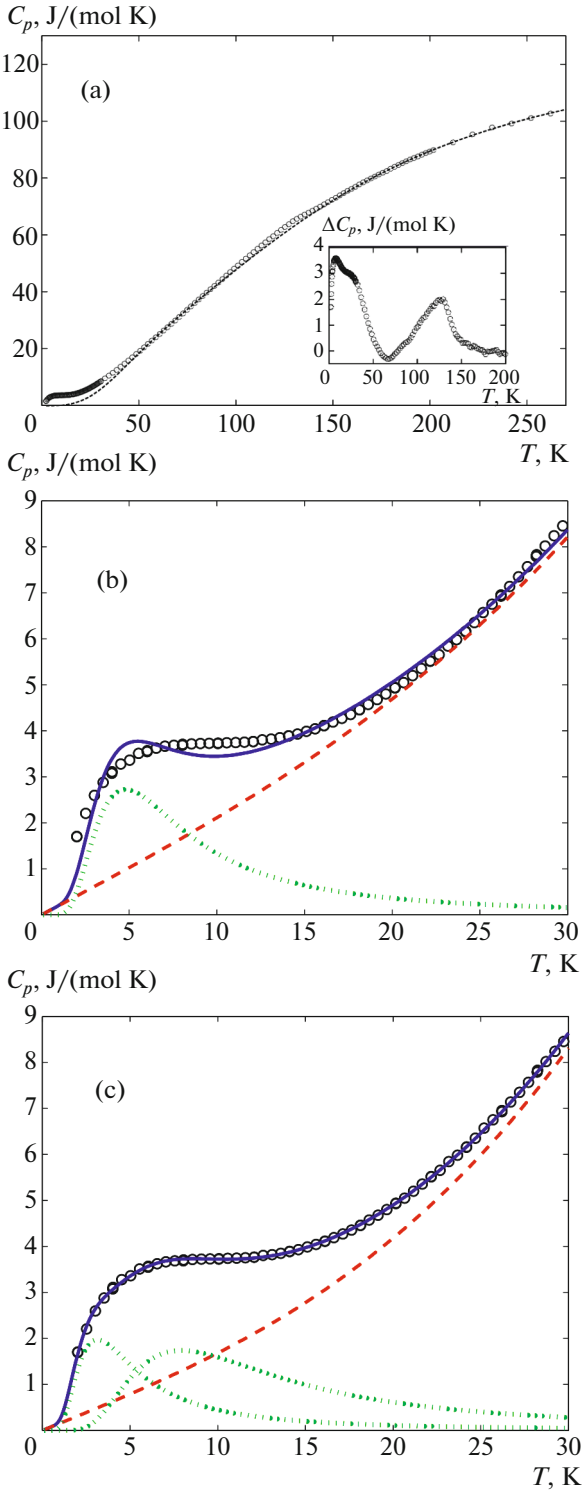

Fig. 5. (Color online) Temperature dependence of the heat capacity C_p of $Gd_{0.4}Sr_{0.6}CoO_{2.85}$ in the temperature range (a) 2–275 K and (b, c) 2–30 K. (open circles) Experimental data, (dashed curve) regular component (lattice and electron) of the heat capacity, (dotted curve) Schottky heat capacity contributions, and (solid curve) sum of the regular component and the Schottky heat capacity contributions.

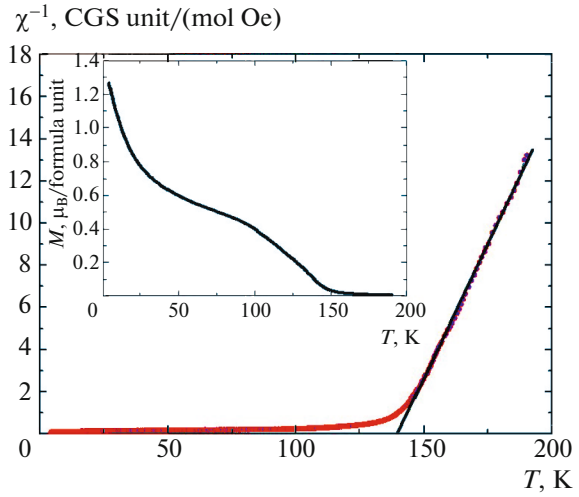

Fig. 6. (Color online) Temperature dependence of the reciprocal magnetic susceptibility of a crystalline $Gd_{0.4}Sr_{0.6}CoO_{2.85}$ sample in a field $H = 500$ Oe. (straight line) Approximation by a linear relation according to the Curie–Weiss law in the temperature range above 150 K ($T_C \approx 138$ K). (inset) Temperature dependence of magnetization in the temperature range under study.

[25] when studying the low-temperature anomaly of the heat capacity of $LaCoO_3$ in a magnetic field, the experimental data from [26–28], and the theoretical concepts in [29]. It should be noted that the splitting $\Delta_1 = 8.3$ K agrees well with the experimental splitting determined by inelastic neutron scattering [28]. The appearance of the second gap is less obvious, since neither Co ions having various charge states (Co^{4+}, Co^{3+}, Co^{2+}) nor, a fortiori, Gd^{3+} and Sr^{2+} ions have the corresponding energy structure of multielectron terms even with allowance for spin–orbit coupling and various crystalline distortions. Our assumption is that the presence of the second energy scale ($\Delta_2 = 21.8$ K) is related to partial hole localization at oxygen in doping. As a result, the incompletely filled $2p^5$ state of oxygen with orbital moment $L = 1$ and spin $S = 1/2$ splits into a doubly degenerate ground state with a total angular moment $J = 1/2$ and a quadruply degenerate excited state with an angular moment $J = 3/2$ because of spin–orbit coupling, and the splitting corresponds to Δ_2 (Fig. 7b). Of course direct measurements and observations are required for a more convincing conclusion. Nevertheless, a powerful argument for this assumption is the fact that the gap $\Delta_2 = 21.8$ K is close to the fine splitting of the energy levels of the sodium atom for the first excited orbit, $\Delta W_{Na} = 24$ K. Since the charge of the oxygen atomic nucleus is lower than the charge of the sodium atomic nucleus, we have $\Delta_2 < \Delta W_{Na}$.

Another interesting finding is that two Schottky anomalies exist only in doped compositions, whereas the plain compositions have only one anomaly corresponding to an energy gap $\Delta_1 \approx 8$ K [25].

4. DISCUSSION AND CONCLUSIONS

The substitution of Sr^{2+} ions for some Gd^{3+} ions in stoichiometric compounds should cause the appearance of holes in the Co($3d$) or O($2p$) state and, hence, the $3d^{6-x}$ or $2p^{6-x/3}$ electron configuration. If the first scenario of hole doping takes place, the properties of the $Gd_{1-x}Sr_xCoO_{3-\delta}$ system are considered in terms of mixing the Co^{3+} and Co^{4+} ion states. At a fixed oxygen nonstoichiometry δ, the charge state of cobalt should monotonically change with concentration x. This approach to structurally ordered $Gd_{0.4}Sr_{0.6}CoO_{2.78}$ should lead to an increase in the

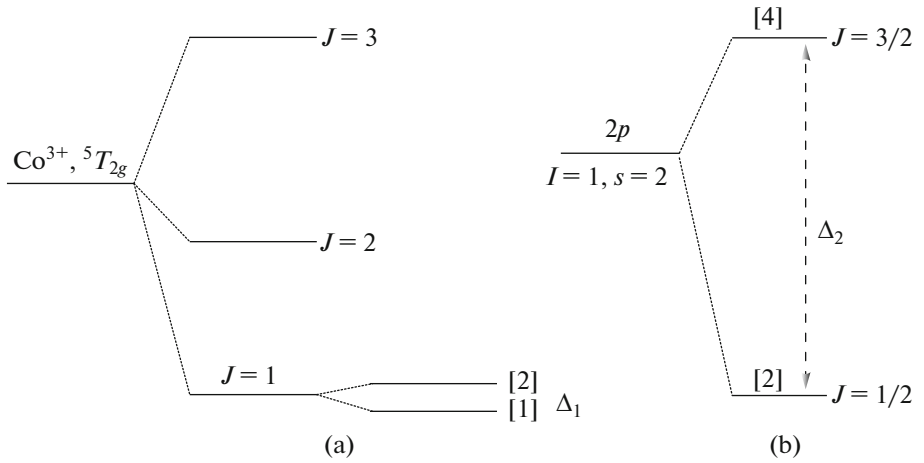

Fig. 7. Set of low-energy multielectron terms for (a) $3d^6$ electron configuration of the Co^{3+} cobalt ion in the crystal field and (b) $2p^5$ electron configuration of the O^{1-} oxygen ion. The numerals in square brackets indicate the degeneracy multiplicity of the terms.

charge state of cobalt to $Co^{3.16+}$, and this approach applied to disordered $Gd_{0.4}Sr_{0.6}CoO_{2.64}$ should bring about a decrease in this state to $Co^{2.88+}$ (instead of Co^{3+} in $GdCoO_3$). If the chemical shift and the charge state of Co are assumed to be linearly related, a change in the valence should induce a visible shift of the absorption edge toward high/low energy. Nevertheless, the experimentally detected shift of the absorption edge in GSC-ord and GSC-dis does not exceed 0.5 eV. Therefore, the charge state of cobalt (Co^{3+}) is thought to remain unchanged in substituted $Gd_{0.4}Sr_{0.6}CoO_{2.64}$ and $Gd_{0.4}Sr_{0.6}CoO_{2.78}$. The XANES spectra are independent of nonstoichiometry and cation ordering/disordering.

Two Schottky anomalies were detected in the low-temperature range of the heat capacity of all substituted samples under study, namely, single-crystal ordered and polycrystalline ordered and disordered samples with various nonstoichiometries. These anomalies are thought to be related to the HS state of the Co^{3+} ions in the pyramidal environment caused by oxygen deficiency and to the magnetic state of oxygen ions induced by the doping-assisted generation of a hole in the 2*p* state.

The unusual results obtained in this work, such as no change in the charge state of cobalt in the $Gd_{0.4}Sr_{0.6}CoO_{3-\delta}$ solid solution, raise new questions about the nature of conduction and magnetism in doped cobaltites, which are still poorly understood.

ACKNOWLEDGMENTS

This work was supported by the Russian Foundation for Basic Research, the Government of the Krasnoyarsk Territory, and Krasnoyarsk Territory Foundation for the Support of Scientific and Research Activity (project nos. 16-42-240413, 16-43-240505); the Council on Grants at the President of the Russian Federation (project nos. SP-1844.2016.1, SP-938.2015.5, NSh-7559.2016.2); and the Russian Foundation for Basic Research (project nos. 17-02-00826, 16-02-00507, 16-32-60049).

REFERENCES

1. N. B. Ivanova, S. G. Ovchinnikov, M. M. Korshunov, I. M. Eremin, and N. V. Kazak, Phys. Usp. **52**, 789 (2009).
2. M. Imada, A. Fujimori, and Y. Tokura, Rev. Mod. Phys. **70**, 1039 (1998).
3. J. Goodenough, Rep. Prog. Phys. **67**, 1915 (2004).
4. S. Maekava, T. Tohyama, S. E. Barnes, S. Ishihara, W. Koshibae, and G. Khaliullin, *Physics of Transition Metal Oxides* (Springer, Berlin, 2004).
5. M. A. Senaris-Rodriguez and J. B. Goodenough, J. Sol. St. Chem. **118**, 323 (1995).
6. M. Itoh, I. Natori, S. Kubota, and K. Motoya, J. Magn. Magn. Mater. **140–144**, 1811 (1995).
7. J. Wu and C. Leighton, Phys. Rev. B **67**, 174408 (2003).
8. T. N. Vasil'chikova, T. G. Kuz'mova, A. A. Kamenev, A. R. Kaul', and A. N. Vasil'ev, JETP Lett. **97**, 34 (2013).
9. M. S. Platunov, V. A. Dudnikov, Yu. S. Orlov, N. V. Kazak, L. A. Solovyov, Ya. V. Zubavichus, A. A. Veligzhanin, P. V. Dorovatovskii, S. N. Vereshchagin, K. A. Shaykhutdinov, and S. G. Ovchinnikov, JETP Lett. **103**, 196 (2016).
10. H. Reitveld, J. Appl. Crystallogr. **2**, 65 (1969).
11. L. A. Solovyov, J. Appl. Crystallogr. **37**, 743 (2004).
12. K. Conder, E. Pomjakushina, A. Soldatov, and E. Mitberg, Mater. Res. Bull. **40**, 257 (2005).
13. O. Haas, R. Struis, and J. M. McBreen, J. Solid State Chem. **177**, 1000 (2004).
14. J. Y. Chang, B. N. Lin, Y. Y. Hsu, and H. C. Ku, Phys. B (Amsterdam, Neth.) **329**, 826 (2003).
15. F. J. Berry, J. F. Marco, and X. Ren, J. Sol. St. Chem. **178**, 961 (2005).
16. M. Sikora, Cz. Kapusta, K. Knizek, Z. Jirak, C. Autret, M. Borowiec, C. J. Oates, V. Prochazka, D. Rybicki, and D. Zajac, Phys. Rev. B **73**, 094426 (2006).
17. V. Kumar, R. Kumar, D. K. Shukla, S. Gautam, K. H. Chae, and R. Kumar, J. Appl. Phys. **114**, 073704 (2013).
18. O. Toulemonde, N. N'Guyen, F. Studer, and A. Traverse, J. Sol. St. Chem. **158**, 208 (2001).
19. Y. Jiang et al., Phys. Rev. B **80**, 144423 (2009).
20. T. Saitoh, T. Mizokawa, A. Fujimori, M. Abbate, Y. Takeda, and M. Takano, Phys. Rev. B **56**, 1290 (1997).
21. S. Medling, Y. Lee, H. Zheng, J. F. Mitchell, J. W. Freeland, B. N. Harmon, and F. Bridges, Phys. Rev. Lett. **109**, 157204 (2012).
22. G. Vanko, J.-P. Rueff, A. Mattila, Z. Nemeth, and A. Shukla, Phys. Rev. B **73**, 024424 (2006).
23. N. Ghosh, U. K. Robler, K. Nenkov, C. Hucho, H. L. Bhat, and K.-H. Muller, J. Phys.: Condens. Matter **20**, 395219 (2008).
24. Z. Hu, Hua Wu, M. W. Haverkort, H. H. Hsieh, H.-J. Lin, T. Lorenz, J. Baier, A. Reichl, I. Bonn, C. Felser, A. Tanaka, C. T. Chen, and L. H. Tjeng, Phys. Rev. Lett. **92**, 207402 (2004).
25. C. He, H. Zheng, J. F. Mitchell, M. L. Foo, R. J. Cava, and C. Leighton, Appl. Phys. Lett. **94**, 102514 (2009).
26. S. Noguchi, S. Kawamata, K. Okuda, H. Nojiri, and M. Motokawa, Phys. Rev. B **66**, 094404 (2002).
27. M. W. Haverkort, Z. Hu, J. C. Cezar, T. Burnus, H. Hartmann, M. Reuther, C. Zobel, T. Lorenz, A. Tanaka, N. B. Brookes, H. H. Hsieh, H.-J. Lin, C. T. Chen, and L. H. Tjeng, Phys. Rev. Lett. **97**, 176405 (2006).
28. A. Podlesnyak, S. Streule, J. Mesot, M. Medarde, E. Pomjakushina, K. Conder, A. Tanaka, M. W. Haverkort, and D. I. Khomskii, Phys. Rev. Lett. **97**, 247208 (2006).
29. Z. Ropka and R. J. Radwanski, Phys. Rev. B **67**, 172401 (2003).

Translated by K. Shakhlevich